Workshop on Material Appearance Modeling
MANER Conference - Material Appearance Network for Education and Research (2024)
J. Y. Hardeberg and H. Rushmeier (Editors)

Real surface measurement and virtual gonioradiometer for road appearance prediction

K. Xu[1] & M. Ribardière[1] & B. Bringier[1] & D. Meneveaux[1]

[1]University of Poitiers – XLIM, Chasseneuil-du-Poitou, France

Abstract

Measuring road appearance in situ requires either very specific hardware difficult to implement, or extracting core samples from used roads. This is why reflectance estimation from virtual samples constructed from non-invasive acquisitions are useful in a wide range of applications. This article proposes an analysis of several combinations for merging geometric and individual reflectance data, in order to estimate the resulting uncertainty, with various distributions.

1. Introduction

Road surfaces have to be carefully designed and managed since they might influence road users behaviour and safety. Unfortunately, accurately measuring their appearance require goniophotometers which operation conditions are not compatible with instant measurement of samples spreads on several kilometers of roads [SJBEM23]. Furthermore, appearance alone is often not the only factor that have to be studied for road safety studies. Several types of data can be generated by road companies and institutions, such as roughness, heightmaps, lab measurements, material composition, measurements from core samples, etc.

This article focuses on the use of two main input data for estimating road surface appearance: (i) height maps and (ii) albedo map. Our goal is to produce a 3D mesh that could be employed in a virtual gonio-reflectometer [XCB*24]. The challenge is to provide a consistent representation of such a mesh in terms of both height and albedo, since the 3D trianglular mesh reconstruction from a height map is not straightfoward, especially when it has to be combined with an albedo map and properly aligned.

We propose to study several merging strategies, with comparisons and analysis, in order to estimate the corresponding uncertainty. Our study also explores the resulting variations when albedo distribution varies. Finally, we provide some preliminary results with some data coming from existing (real) road surfaces.

2. Surface acquisition

Accurately acquiring the detailed components of a surface for understanding its appearance requires individual representations of geometry, colorimetry, and specular reflexion parameters. Many devices have been proposed in the literature for recovering geometry, for instance relying on Time of Flight (ToF) [KBKL09] or wave interference [Mal07]. Anyway, estimating the albedo requires at least an additional photographic sensor [TTP22]. The representation of a complete virtual surface finally needs a precise matching between these components (geometry, colorimetry, specular parameters). This step is actually complex to carry out, as the recovered information does not share the same spatial resolution, and acquisitions correspond to different points of view. This article proposes an experiment, based on photometric stereo, that can be considered as reliable for simultaneously acquiring the geometry and color of a rough surface, because all the images are acquired from a single viewpoint. A 3D geometric mesh is reconstructed from per-pixel estimated normal through an integration process [PJBK23]. Even though estimated geometry and albedo are per-pixel aligned, the construction of a 3D mesh with one reflectance value per triangle is not straightforward.

Our stereo-photometric device consists of 11 lights distributed over two rings and a color camera with a 75 mm focal-length lens. It is a lightweight system, designed for being employed in various types of environments (typically roads or archeological sites). The acquired surfaces size can be 146 by 106.9 mm, and the resulting resolution corresponds to about 71 μm. The sensitivity of the red, green and blue channels of the camera is calibrated, and high dynamic range imaging ensures accurate results. Figure 4 shows a 3D visualization of the five surfaces acquired with our device and used in our study.

3. From measurement to digital surface

The resulting 3D mesh and the acquired HDR reflected radiance measured per image pixel need to be combined in order to be employed in the ray-tracing process embedded in our virtual gonio-reflectometer. We propose to study the difference between two different merging strategies, given that ray-tracing techniques may

DOI: 10.2312/mam.20241180

employ reflectance values either per face, or per vertex (and use interpolation), see Figure 1.

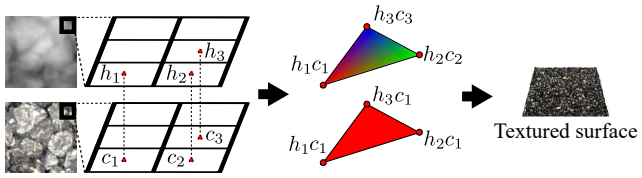

Figure 1: *(a) The acquired height and color (albedo) value for each pixel p are denoted as h_p and c_p respectively. Height values are used to generate a triangular mesh where albedo values are associated to each vertex. (b) Two different solutions are proposed for mapping colors, which can be either interpolated per vertex (barycentric) or constant on the whole triangle, determined by one of its vertices.*

None of these approaches can be considered as better or worse strictly speaking. The value associated with a single vertex is not really representative of the entire facet, but the acquisition system does either not actually produce a mesh aligned with triangles that would correspond to constant mono-reflectance characteristics. We compare the effects of these two approaches on the final output BRDFs in Section 5.

4. Virtual gonioradiometer

Dong and al. [DWMG16] suggest a profilometric measurement system to represent the normal distribution function and therefore estimate the BRDF. Unfortunately, for surfaces composed of several materials, this approach cannot be applied. Our simulation system rather mimics a real gonioradiometer. It contains a series of directional light sources, capable of emitting a mono-spectral band collimated ray and grazing angles become virtually manageable (the polar angle θ_i is from 0° to 90° without any restriction). The virtual surface is represented using a triangular mesh, illuminated from one fixed direction $\mathbf{i}$ at a time. The sensor is designed as a uniformly divided hemisphere [BB12], as illustrated in the left of Figure 2 (i.e., iso-solid angle and same aspect ratio for all cells to mitigate acquisition bias).

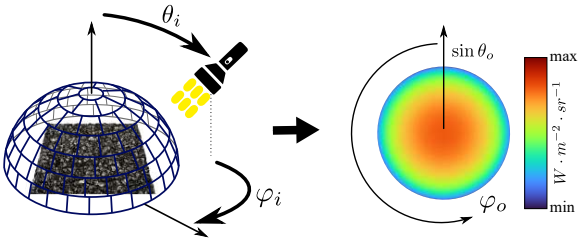

Figure 2: *Our virtual gonioradiometer and the color coded BRDF representation used in this article.*

The lighting simulation process uses path tracing [PJH23], casting rays from the light source toward the surface. The final output is a cosine-weighted BRDF [XCB*24], projected onto the XY plane for display, illustrated in the right of Figure 2. During the ray-tracing process, the reflectance value associated with a hit point is estimated using one of the two strategies decribed above.

5. Results

This article illustrates the results obtained for 5 road surfaces (Section 5), with a Lambertian assumption. Each surface is defined by a 3D mesh and an albedo map. We also conducted a test with a synthetic surface with strong colors in order to examine how correlation between albedo and height affects the BRDF (Section 5). All our results can be considered convergent (the RMSE remains always less than 0.002 even with an increase of the number of samples). We also considered different polar angles ($\phi_i = \{0^\circ, 30^\circ, 60^\circ, 90^\circ\}$, $\theta_i = \{45^\circ, 80^\circ\}$), and found that the RMSE between the sensor images for a given polar angle θ_i and varying ϕ_i was less than 0.02. Thus, the given road surfaces exhibit only isotropic properties and in the subsequent results, only one BRDF side is presented ($\phi_o = [0^\circ, 180^\circ]$).

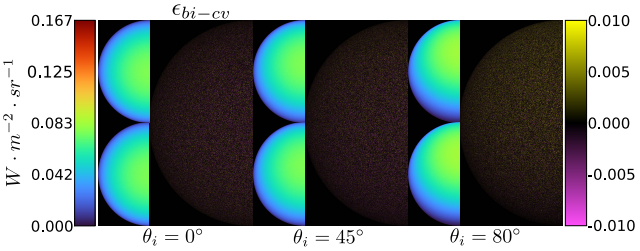

Figure 3: *Impact of color mapping approaches on the output BRDF, under various incident polar angles (θ_i). In each subplot (columns), BRDF values are illustrated on the left: (top) using the interpolation mapping, denoted as f_{bi}, and (bottom) using a constant value mapping, denoted as f_{cv}. The difference values are illustrated with false colors images on the right, $\epsilon_{bi-cv} = f_{bi} - f_{cv}$.*

First, we found that the mapping strategies discussed in Section 3 have only little influence on the final estimated BRDF (Section 5), regardless of the considered incident direction. Even with BRDF differences increased by a factor of $n = 100$, the difference images primarily exhibit noise, making it challenging to discern any clear patterns. The RMSE, computed from BRDF values in the images, is below 0.003. However, definitive conclusions require further investigations we will address in future work. For instance the case of non lambertian assumptions also has to be considered. From these first results, and for the sake of conciseness, the next analysis is presented using constant mapping (without interpolation).

Although road surfaces are considered in this study as composed of Lambertian microfacets, the global appearance depends on the observation direction (Figure 4). Back-reflection increases as the incident direction approaches grazing angles. In order to study this effect, and ensure it is due to the road surface's micro-geometric structure, we have set a diffuse material with a uniform albedo set to 1 on the geometry of road surface type L2. The same recto-reflection phenomenon can be observed (Figure 4), attesting that the micro-geometric structure of road surface cannot be ignored. Existing microfacet models could simulate such a back-reflection

[ON94, MBT*18] effect but their validity in cases where the characteristics of the micro-facets vary along the surface, as is the case for road surfaces, has not been studied yet, to the best of our knowledge.

Real road surface materials are always composite and the components distribution is often height-correlated (e.g., gravel upper layer, asphalt lower layer). We conducted another experiment using a triangular mesh of a $4 \times 4\text{mm}^2$, generated from an isotropic Beckmann NDF (roughness $\alpha = 0.25$) and applied both height-correlated and uncorrelated albedo maps (Figure 6). As expected, the resulting BRDF shows a significant height-dependence: when the incident angle becomes grazing, the upper layer's contribution to the BRDF slightly increases, while the lower layer's decreases. Thus, observing the surface at grazing angles, the upper layer's contribution sharply increases, while the lower layer's sharply decreases, as demonstrated by the halo effect of the differences (ϵ_{hc-huc}) between BRDFs in red and blue channels in Figure 6. Such effects can be simulated with recent works of D'Eon *et al.* [dBWZ23] or Lucas *et al.* [LRPB24] but their adaptation in road surface appearance, with complex correlation between component's height and BSDF, has yet to be investigated.

6. Conclusion

The preliminary experiments presented in this paper have already unveiled fundamental properties of road surface materials, specifically, pronounced back-reflection and notable height correlation. Moreover, the consistent manifestation of distinct reflective characteristics at grazing angles is particularly significant. In practice, drivers frequently observe road surfaces from grazing angles, emphasizing the importance of this spot.

In the future, several critical tasks lie ahead. First, enhancing the accuracy of material color acquisition is paramount, as it will improve the fidelity of our simulations. Second, developing more precise methods for geometric and color mapping will enable more accurate representation of road surface materials. Finally, adapting a SVBRDF representation from a micro-geometric perspective is essential. It will provide more accurate road surface rendering support for practical applications, such as upgrading urban public lighting systems.

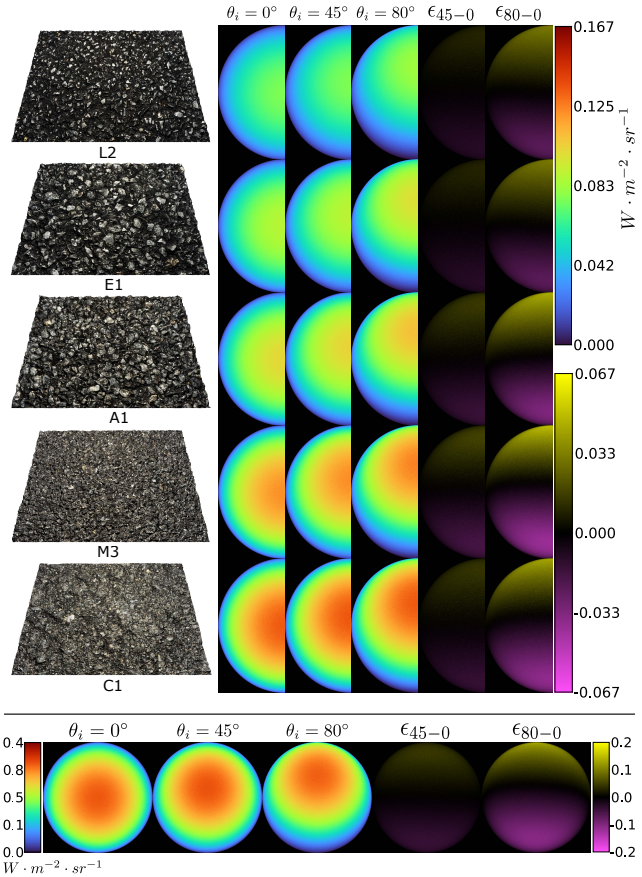

Figure 4: *(left part) Visualization of five different 3D road surfaces reconstructed by our photometric stereo device and (right part) the BRDF of these surfaces under various incident polar angles (θ_i): The first three columns correspond to the resulting BRDF at different incident angles, denoted as f_0, f_{45}, and f_{80}; The last two columns illustrate the corresponding differences, $\epsilon_{45-0} = f_{45} - f_0$ and $\epsilon_{80-0} = f_{80} - f_0$. The row below presents the results obtained using a constant lambertian albedo = 1 on the L2 surface.*

7. Acknowledgement

This research was funded, in whole or in part, by the French National Research Agency (ANR) under the REFLECTIVITY project : ANR-22-CE22-0006.

References

[BB12] BECKERS B., BECKERS P.: A general rule for disk and hemisphere partition into equal-area cells. *Computational Geometry 45*, 7 (2012), 275–283. 2

[dBWZ23] D'EON E., BITTERLI B., WEIDLICH A., ZELTNER T.: Microfacet theory for non-uniform heightfields. In *SIGGRAPH 2023 Conference Papers* (New York, NY, USA, 2023), Association for Computing Machinery. 3

[DWMG16] DONG Z., WALTER B., MARSCHNER S., GREENBERG D. P.: Predicting appearance from measured microgeometry of metal surfaces. *ACM Transactions on Graphics 35*, 1 (dec 2016). 2

[KBKL09] KOLB A., BARTH E., KOCH R., LARSEN R.: Time-of-flight sensors in computer graphics (state-of-the-art report). In *Proceedings of Eurographics 2009 - State of the Art Reports* (2009), The Eurographics Association, pp. 119–134. 1

[LRPB24] LUCAS S., RIBARDIÈRE M., PACANOWSKI R., BARLA P.: A Fully-correlated Anisotropic Micrograin BSDF Model. *ACM Transactions on Graphics 43*, 4 (July 2024), 111. 3

[Mal07] MALACARA D.: *Optical Shop Testing, 3rd ed.* Wiley, 2007. 1

[MBT*18] MENEVEAUX D., BRINGIER B., TAUZIA E., RIBARDIÈRE M., SIMONOT L.: Rendering rough opaque materials with interfaced lambertian microfacets. *IEEE Transactions on Visualization and Computer Graphics 24*, 3 (2018), 1368–1380. 3

[ON94] OREN M., NAYAR S. K.: Generalization of Lambert's reflectance model. In *ACM SIGGRAPH* (july 1994), pp. 239–246. 3

[PJBK23] PROUTEAU N., JOUBERT C., BRINGIER B., KHOUDEIR M.: Continuous material reflectance map for deep photometric stereo. *J. Opt. Soc. Am. A 40*, 4 (Apr 2023), 792–802. 1

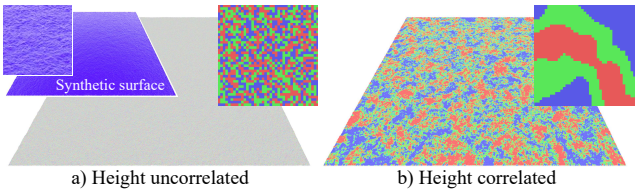

Figure 5: *Synthetic surface with a triangular mesh, generated from a given normal distribution function. a) With a random colored albedo map; b) With a height-correlated colored albedo, the upper layer being red, the bottom layer blue, and the middle layer green. Note that the color distributions are the same in both maps.*

[PJH23] PHARR M., JAKOB W., HUMPHREYS G.: *Physically based rendering: From theory to implementation*. MIT Press, 2023. 2

[SJBEM23] SAINT JACQUES E., BRÉMOND R., EYMOND F., MORVAN K.: Investigating the evolution of road surface descriptors according to observation angles using a database of the reflection properties of urban materials. The 30th Quadriennal Session of the CIE, Sept. 2023. 1

[TTP22] TYCHOLA K. A., TSIMPERIDIS I., PAPAKOSTAS G. A.: On 3d reconstruction using rgb-d cameras. *Digital 2*, 3 (2022), 401–421. 1

[XCB*24] XU K., CAVALIER A., BRINGIER B., RIBARDIÈRE M., MENEVEAUX D.: Virtually measuring layered material appearance. *J. Opt. Soc. Am. A 41*, 5 (2024), 959–968. 1, 2

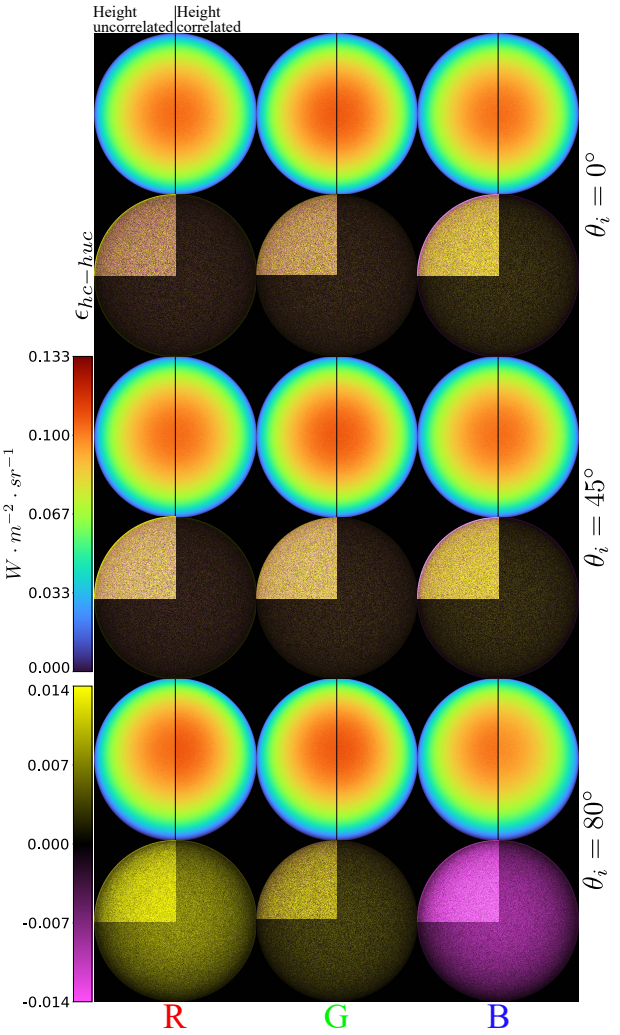

Figure 6: *BRDFs obtained from the surfaces depicted in Figure 5, with different incident polar angles (θ_i). The values obtained with the height-uncorrelated map is denoted as f_{huc}, while those obtained using the height-correlated map is denoted as f_{hc}. Their difference is given by $\epsilon_{hc-huc} = f_{hc} - f_{huc}$. The top-left differences are magnified by a factor of $n = 5$, in order to better observe the significant height-correlation on BRDF at grazing angles.*